Quantum reflection by Casimir−van der Waals potential tails

Harald Friedrich,* Georg Jacoby, and Carlo G. Meister

Physik-Department, Technische Universität München, 85747 Garching, Germany

We study the reflectivity of Casimir−van der Waals potentials, which behave as $-C_4/r^4$ at large distances and as $-C_3/r^3$ at small distances. The overall behavior of the reflection amplitude R depends crucially on the parameter $\rho = \sqrt{2M}\,C_3/(\hbar\sqrt{C_4})$ which determines the relative importance of the $-1/r^3$ and the $-1/r^4$ parts of the potential. Near threshold, $E = \hbar^2 k^2/(2M) \rightarrow 0$, the reflectivity is given by $|R| \sim \exp(-2bk)$, with b depending on ρ and the shape of the potential at intermediate distances. In the limit of large energies, $\ln|R|$ is proportional to $-k^{1/3}$ with a known constant of proportionality depending only on C_3. For small values of ρ, the reflectivity behaves as for a homogeneous $-1/r^3$ potential in the whole range of energies and does not depend on C_4 or the shape of the potential beyond the $-1/r^3$ region. For moderate and large values of ρ, the reflectivity depends on C_4 and on the potential shape. For sufficiently large values of ρ, which are ubiquitous in realistic systems, there is a range of energies beyond the near-threshold region, where the reflectivity shows the high-energy behavior appropriate for a homogeneous $-1/r^4$ potential, i.e., $\ln|R|$ is proportional to $-\sqrt{k}$ with a proportionality constant depending only on C_4. This conspicuous and model-independent signature of the Casimir effect is illustrated for the reflectivities of neon atoms scattered off a silicon surface, which were recently measured by Shimizu [Phys. Rev. Lett. **86**, 987 (2001)].

I. INTRODUCTION

A particle moving through a classically allowed region can be reflected by a potential without reaching a classical turning point. Such ''quantum reflection'' can, e.g., be caused by the long-range part of an atom-surface interaction, and it is an important effect, because it reduces the probability for the incident atom to come close enough to interact with the shorter-ranged forces and to be inelastically scattered or adsorbed. For potential tails vanishing faster than $1/r^2$, the quantum reflection probability approaches unity as the velocity of the projectile approaches zero, so it is always non-negligible at sufficiently low energies [1–3].

The current intense activity on cold atoms has made quantum reflection by attractive potential tails a topic of considerable interest [4]. The electrostatic interaction of a polarizable atom and a surface is a van der Waals potential proportional to $-1/r^3$ [5]. At very large distances, however, retardation becomes important and the potential becomes proportional to $-1/r^4$ as described by Casimir and Polder in 1948 [6]. The retarded van der Waals potential is just one manifestation of the ''Casimir effect'' which describes forces induced by the zero-point energy of the quantized electromagnetic field. A detailed review of the state of the art in the theoretical understanding and experimental investigations of the Casimir effect has just been published by Bordag *et al.* [7]. The Casimir effect is experimentally observable in quantum reflection by a retarded van der Waals potential tail as recently demonstrated by Shimizu [8], who showed that the inclusion of the retardation effects is necessary in order to explain the observed reflectivities.

In some applications, e.g., atomic mirrors constructed via laser beams totally reflected on the inside of a prism [9,10],

the atom-surface interaction contains not only the Casimir–van der Waals contribution, but it can also contain a short-ranged repulsive part coming from the evanescent electric field outside the prism. The short-ranged repulsive term and the attractive Casimir–van der Waals term can combine to produce a potential barrier. In such cases, the energy dependence of the reflection probability is close to the classically predicted sharp step at the barrier energy, and the quantum effects mainly smooth this sharp-step behavior.

The aim of this paper is to study quantum reflection by Casimir–van der Waals potentials in detail and to investigate how the behavior of the reflectivity as a function of energy depends on the strength parameters and the shape of the potential. We focus on purely attractive potential tails, where reflection is forbidden classically and is a quantum-mechanical effect at all energies.

In Sec. II we briefly review a few general aspects of quantum reflection, and we show how the reflectivity depends on energy in the case of homogeneous potential tails. In Sec. III, we generalize this theory to Casimir–van der Waals potentials, and we discuss the energy dependence of the reflectivity expected for various values of the parameters determining the strength of the potential in the short-distance and the long-distance regimes. The influence of the shape of the potential in between the two limits is illustrated with the help of three realistic models. In Sec. IV, we show how recent data of Shimizu on quantum reflection of neon atoms by a silicon surface [8] fit in to the expectations presented in Sec. III.

II. GENERAL ASPECTS OF QUANTUM REFLECTION, HOMOGENEOUS TAILS

The unambiguous definition of amplitudes and probabilities for transmission through a localized region of coordinate space implies that there are unidirectional solutions of the equations of motion on either side of this region. Unidirec-

---

*Email address: harald.friedrich@ph.tum.de

tional solutions of the Schrödinger equation are provided by the appropriate WKB wave functions [11],

$$\psi_{\text{WKB}}(r) \propto \frac{1}{[p(r)]^{1/2}} \exp\left(\pm \frac{i}{\hbar} \int^r p(r')dr' \right), \qquad (1)$$

as long as these WKB wave functions are accurate approximations of the exact solutions. In Eq. (1), $p(r)$ is the local classical momentum of a particle of mass M moving in a potential $V(r)$,

$$p(r) = \sqrt{2M[E-V(r)]}, \qquad (2)$$

and the condition for applicability of the WKB approximation is essentially that the local de Broglie wavelength $2\pi\hbar/p(r)$ should vary slowly with the coordinate r. More precisely (see [11], p. 48 of [12]),

$$|B(r)| \ll 1,$$

$$B(r) = \frac{\hbar^2}{[p(r)]^{3/2}} \frac{d^2}{dr^2}[p(r)^{-1/2}] = \hbar^2 \left(\frac{3}{4} \frac{(p')^2}{p^4} - \frac{1}{2} \frac{p''}{p^3} \right). \qquad (3)$$

The WKB wave functions (1) are poor approximations when $B(r)$, the "badlands function," is significantly nonzero. They accurately approximate solutions to the Schrödinger equation when the condition (3) is fulfilled. This is clearly the case if the dependence of V on r is negligible, but Eq. (3) is also increasingly well fulfilled towards small r values if $V(r)$ is more singular than $1/r^2$ at the origin, $r=0$. For potential tails proportional to $1/r^\alpha$, $B(r)$ becomes independent of energy and proportional to $r^{\alpha-2}$ for small r values [see the Appendix, Eq. (A6)]. For $\alpha>2$, the WKB approximation thus becomes increasingly accurate as $r \to 0$, and, for nonzero energies $E \neq 0$, also for $r \to \infty$; i.e., the badlands where Eq. (3) is not fulfilled lie between two WKB regions, one for small r and one for large r, where the Schrödinger equation has unidirectional solutions. It is hence meaningful to speak of transmission through or reflection by the badlands in the tail of the potential, even when there is no potential barrier and there are no classical turning points.

A remarkable feature of quantum reflection by a potential tail falling off faster than $1/r^2$ is that the reflection probability $|R|^2$ always goes to unity at threshold $E=0$. Regardless of whether or not there is a potential barrier, the absolute value of the reflection amplitude (which we shall call the "reflectivity") has the universal behavior

$$|R| \overset{k \to 0}{\sim} 1-2bk, \qquad (4)$$

where k is the wave number defining the asymptotic kinetic energy, $E = \hbar^2 k^2/(2M)$. The length b in (4) is a "tail parameter" which depends only on the potential beyond the inner WKB region; it also determines the near-threshold quantization rule and level density just below threshold and can be derived from the zero energy solutions of the Schrödinger equation in the tail region as described in detail in [13]. For

potential tails falling off faster than $1/r^2$, there are, for $E=0$, two linearly independent solutions of the Schrödinger equation behaving asymptotically ($r \to \infty$) as $\psi_0 \sim 1$, $\psi_1 \sim r$. Following these solutions to smaller r values allows them to be written as

$$\psi_{0,1}(r) = D_{0,1}[p_0(r)]^{-1/2} \cos\left[\frac{1}{\hbar} \int_r^\infty p_0(r')dr' - \frac{1}{2}\phi_{0,1} \right] \qquad (5)$$

in the inner WKB region; p_0 is the local classical momentum (2) at $E=0$. The length parameter b is given [13] by the difference $\phi_0-\phi_1$ of the phases and the ratio D_1/D_0 of the amplitudes appearing in Eq. (5),

$$b = \frac{D_1}{D_0} \sin\left(\frac{\phi_0-\phi_1}{2} \right). \qquad (6)$$

Consider a homogeneous potential tail,

$$V_\alpha(r) = -\frac{C_\alpha}{r^\alpha} = -\frac{\hbar^2}{2M} \frac{(\beta_\alpha)^{\alpha-2}}{r^\alpha}, \qquad \alpha>2. \qquad (7)$$

Here we have introduced the length parameter β_α, which is related to the potential strength C_α via Planck's constant and sets the scale on which to expect quantum effects. The Schrödinger equation with the potential (7) can be rescaled so that it only contains one parameter, namely $k\beta_\alpha$, so all properties of its solutions can only depend on $k\beta_\alpha$. Since $\alpha>2$, $k\beta_\alpha \to \infty$ corresponds to the semiclassical limit and $k\beta_\alpha \to 0$ corresponds to the anticlassical or extreme quantum limit, see Refs. [14,15] and p. 322 of Ref. [12]. The zero energy solutions of the Schrödinger equation with the potential (7) are Bessel functions of order $\pm 1/(\alpha-2)$, and the length b as given by Eq. (6) is [13,15–17],

$$b = \beta_\alpha \frac{\sin[\pi/(\alpha-2)]}{(\alpha-2)^{2/(\alpha-2)}} \frac{\Gamma\left(1-\frac{1}{\alpha-2}\right)}{\Gamma\left(1+\frac{1}{\alpha-2}\right)} \overset{\text{def}}{=} b_\alpha. \qquad (8)$$

In particular,

$$b_3 = \pi\beta_3 \quad \text{for} \quad \alpha=3, \quad b_4=\beta_4 \quad \text{for} \quad \alpha=4,$$

$$\text{and} \quad b_\alpha \sim (\pi/\alpha)\beta_\alpha \quad \text{for} \quad \alpha \to \infty. \qquad (9)$$

A further useful example is the exponential potential,

$$V_{\text{exp}}(r) = -\frac{\hbar^2}{2M}(K_0)^2 \exp(-r/\beta_{\text{exp}}), \qquad (10)$$

where the "inner" WKB region is actually $r \to -\infty$, and we have $b = \pi\beta_{\text{exp}}$. The Schrödinger equation with the potential (10) can be solved analytically at all energies [18], and the reflectivity is [11,16]

$$|R_{\text{exp}}| = \exp(-2\pi k\beta_{\text{exp}}). \qquad (11)$$

Near threshold, the leading behavior of the exponential in Eq. (11) is indistinguishable from the linear behavior (4), but the exponential behavior (11) is valid for all (positive) energies. For other potentials, the behavior of $|R|$ significantly above threshold is not so simple, but numerical calculations have shown [19] that replacing (4) with the corresponding exponential

$$|R| \overset{k \to 0}{\sim} \exp(-2bk) \tag{12}$$

reproduces the next-to-leading behavior of $|R|$ quite well in a number of cases, including homogeneous potential tails (7).

For potential tails vanishing faster than $1/r^2$, the high-energy limit is the semiclassical limit [15], and the reflection amplitudes vanish in this limit. The energy dependence of the reflection amplitudes at large energies depends on details of the potential, and there is no universally valid formula such as (4) or (12) for the low-energy limit. If there is a discontinuity in one of the derivatives of the potential, then the lowest order n for which this occurs dominates the reflectivity, which vanishes as $\hbar^n$ in the semiclassical limit. When all derivatives of the potential are continuous, the reflectivity usually vanishes exponentially.

For large energies, the badlands function (3) becomes smaller and smaller and more and more localized in the region where the absolute value of the potential energy is roughly equal to the total energy (see the Appendix). Prokovskii *et al.* [20,21] analyzed an approximation of the reflection amplitude based on a perturbative treatment of the badlands function $B(r)$ (see also Maitra and Heller [22]), and they derived the asymptotic formula

$$R \sim -i \exp\left(\frac{2i}{\hbar} \int^{r_t} p(r) dr\right), \tag{13}$$

where r_t is the complex turning point with the smallest (positive) imaginary part.

For the exponential potential (10), the complex turning points are given by

$$\frac{r_{t,\exp}^{(n)}}{\beta_{\exp}} = -\ln\left(\frac{k^2}{(K_0)^2}\right) + (2n+1)i\pi, \quad n = 0, \pm 1, \pm 2, \ldots, \tag{14}$$

and $n = 0$ corresponds to the one with the smallest positive imaginary part. Taking the integral in the exponent on the right-hand side of (13) over the path $r = -\ln[k^2/(K_0)^2]\beta_{\exp} + \xi i\pi\beta_{\exp}$, $\xi = 0 \to 1$, yields $R \sim -i \exp(-2\pi k\beta_{\exp})$, which agrees with the exact result (11) for $|R_{\exp}|$ — at all energies [19].

For a homogeneous potential tail (7) with integer power α, there are altogether α complex turning points located at $(-1)^{1/\alpha} r_0$, where r_0 is the point at which the absolute value of the potential energy, $|V_\alpha(r_0)|$, is equal to the asymptotic kinetic energy, i.e., the total energy $E = \hbar^2 k^2/(2M)$,

$$r_0 = k^{-2/\alpha}(\beta_\alpha)^{1-2/\alpha}. \tag{15}$$

TABLE I. The coefficients B_α, which are given by Eq. (19) and appear before $a_\alpha = (k\beta_\alpha)^{1-2/\alpha}$ in the exponents describing the high-energy behavior (17) of the reflectivities of homogeneous potential tails.

α	3	4	5	6	7	8
B_α	2.24050	1.69443	1.35149	1.12025	0.95450	0.83146

The complex turning point with the smallest positive imaginary part is

$$r_{t,\alpha} = \left[\cos\left(\frac{\pi}{\alpha}\right) + i \sin\left(\frac{\pi}{\alpha}\right)\right] k^{-2/\alpha}(\beta_\alpha)^{1-2/\alpha}. \tag{16}$$

In the integral in the exponent in Eq. (13), a path along the real axis gives real contributions and only affects the phase of the reflection amplitude. Integrating along a path $r = \text{Re}(r_{t,\alpha}) + i\xi \text{Im}(r_{t,\alpha})$, $\xi = 0 \to 1$, yields the following expression for the absolute value of the reflection amplitude R_α (at high energies):

$$|R_\alpha| \sim \exp(-B_\alpha k r_0) = \exp(-B_\alpha a_\alpha). \tag{17}$$

Here we have introduced the abbreviation

$$a_\alpha = k r_0 = (k\beta_\alpha)^{1-2/\alpha}. \tag{18}$$

The coefficients B_α appearing before the k-dependent term a_α in the exponent in Eq. (17) are

$$B_\alpha = 2 \sin\left(\frac{\pi}{\alpha}\right) \text{Re}\left\{\int_0^1 \sqrt{1 + \left[\cos\left(\frac{\pi}{\alpha}\right) + i\xi \sin\left(\frac{\pi}{\alpha}\right)\right]^{-\alpha}} \, d\xi\right\}. \tag{19}$$

The numerical values of the coefficients B_α are listed in Table I for $\alpha = 3, \ldots, 8$. For large α, the real part of the integral in Eq. (19) becomes unity and $B_\alpha \sim 2\pi/\alpha$.

An alternative and very simple approach to derive an approximation for the reflectivity of homogeneous potential tails is based on the idea of comparison potentials. At energy $E = \hbar^2 k^2/(2M)$, the region in coordinate space important for reflection is around the value r_0 defined by Eq. (15). At $r = r_0$, the depth of the potential is $V_\alpha(r_0)$ and the derivative is $(-\alpha/r_0)V_\alpha(r_0)$. The exponential potential (10) has the depth $V_{\exp}(r_0)$ and the derivative is $(-1/\beta_{\exp})V_{\exp}(r_0)$. Depth and derivative of the exponential potential can be made to agree with depth and derivative of the homogeneous potential at r_0 if the width parameter $\beta_{\exp}$ of the exponential is chosen as

$$\beta_{\exp} = r_0/\alpha. \tag{20}$$

An approximation to the reflectivity of the homogeneous potential is obtained by taking the (exact) expression (11) for the reflectivity of the exponential potential for this value of $\beta_{\exp}$,

$$|R_\alpha| \approx \exp(-2\pi kr_0/\alpha) = \exp\left(-\frac{2\pi}{\alpha}(k\beta_\alpha)^{1-2/\alpha}\right).$$

$$(21)$$

Here we have inserted the right-hand side of Eq. (18) for kr_0. The approximation (21) contains the same power of $k\beta_\alpha$ in the exponent as does Eq. (17), and the coefficient in the exponent corresponds to the large-α limit of the coefficients B_α.

In the limit of large powers, $\alpha \to \infty$, the expressions (17) and (21) agree with the near-threshold behavior (12)

$$|R_\alpha| \overset{k\to 0}{\sim} \exp(-2kb_\alpha) \qquad (22)$$

when the large-α limit for the length parameter b_α is inserted according to Eq. (9). For finite powers α, the expressions (17) and (21) are clearly wrong near threshold, because their exponents depend on a power of $k\beta_\alpha$ which is smaller than unity. This dependence seems correct at high energies, however, and numerical results below strongly support Eq. (17) as the correct expression for the high-energy behavior of the reflectivity of homogeneous potential tails.

In Fig. 1, we show the (numerically calulated) reflectivities $|R_\alpha|$ of homogeneous potential tails for powers $\alpha = 3, \dots, 6$. In part (a) of the figure, we plot $\ln(|R_\alpha|)$ as functions of $k\beta_\alpha$. The near-threshold behavior (22) manifests itself in a linear decrease of $\ln|R_\alpha|$ for small values of $k\beta_\alpha$, and the gradient is $-2b_\alpha/\beta_\alpha$, with the b_α's as given by Eq. (8). This linear decline slows down towards higher energies, however, where we expect $-\ln(|R_\alpha|)$ to be proportional to $a_\alpha = (k\beta_\alpha)^{1-2/\alpha}$ according to Eq. (17). This is in fact borne out by the numerical calculations, as illustrated in part (b) of Fig. 1, where we have plotted $\ln(|R_\alpha|)$ as functions of a_α. The straight solid lines show the asymptotic behavior predicted by Eq. (17); their slope is determined by the coefficients B_α given in Eq. (19) and Table I. The convergence of the numerically calulated reflectivities to the straight lines predicted by Eq. (17) seems obvious. The behavior predicted by Eq. (21) would also corresponds to straight lines in part (b) of Fig. 1, but the gradients $-2\pi/\alpha$ differ from those of Eq. (17) by up to 8% (for $\alpha = 4$) and clearly do not correctly describe the high-energy behavior of the reflectivities.

The reflectivities $|R_\alpha|$ are monotonously decreasing functions of $k\beta_\alpha$. This means that, for a given energy (fixed value of k) the reflectivity increases with decreasing β_α. Making the potential weaker increases the quantum reflectivity at a given energy E. At the same time, the region where reflection is essentially generated, i.e., where the absolute value of the potential is equal to E, moves to smaller r values according to Eq. (15).

The behavior of $\ln(|R_\alpha|)$ changes from proportionality to $k\beta_\alpha$ at small energies to proportionality to $(k\beta_\alpha)^{1-2/\alpha}$ at large energies. Writing

$$|R| = \exp[-Bk^\mu] \qquad (23)$$

and taking (natural) logarithms leads to

(a)

(b)
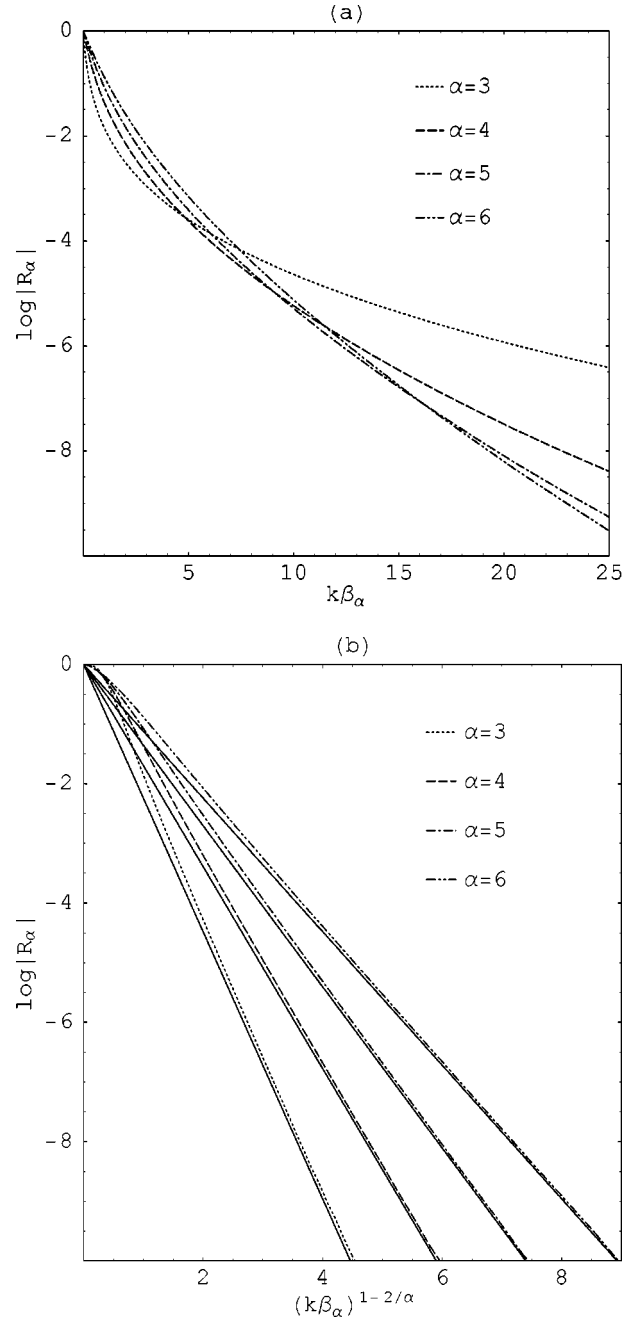
FIG. 1. Reflectivities $|R_\alpha|$ of homogeneous potential tails (7) for powers α ranging from 3 to 6. The natural logarithms $\ln|R_\alpha|$ of the reflectivities are plotted as functions of $k\beta_\alpha$ in part (a) of the figure and as functions $a_\alpha = (k\beta_\alpha)^{1-2/\alpha}$ in part (b).

$$\ln(-\ln|R|) = \ln B + \mu \ln k, \qquad (24)$$

so the power μ of k appearing in the exponent is best exposed by plotting $\ln(-\ln|R|)$ as a function of $\ln k$, or more appropriately for the homogeneous potential (7), as function of $\ln(k\beta_\alpha)$. This has been done in Fig. 2 for the numerically calculated reflectivities $|R_\alpha|$ already shown in Fig. 1. For large negative values of $\ln(k\beta_\alpha)$, the graphs approach straight lines of unit gradient, whose intercept with the ordinate is $\ln(2b_\alpha/\beta_\alpha)$, see Eq. (8). For large positive values of
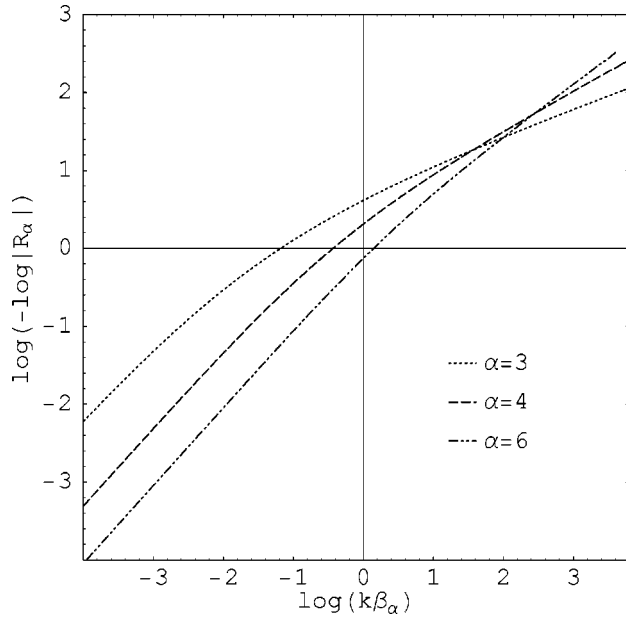
FIG. 2. Reflectivities $|R_\alpha|$ of homogeneous potential tails (7) for the powers $\alpha = 3$, 4, and 6. Here we plot $\ln(-\ln|R_\alpha|)$ as functions of $\ln(k\beta_\alpha)$. For large negative values of $\ln(k\beta_\alpha)$, the curves approach straight lines of unit gradient whose intercepts with the ordinate give the logarithms of $2b_\alpha/\beta_\alpha$, see Eq. (8). For large positive values of $\ln(k\beta_\alpha)$, the curves approach straight lines of gradient $1 - 2/\alpha$ whose intercepts with the ordinate yield the logarithms of the coefficients B_α in Eq. (19), see Table I.

$\ln(k\beta_\alpha)$, the graphs approach straight lines of gradient $1 - 2/\alpha$, whose intercept with the ordinate gives the coefficient $\ln(B_\alpha)$, see Eq. (19), Table I.

III. CASIMIR–VAN DER WAALS POTENTIAL TAILS

The Casimir–van der Waals potential between a spherically symmetric ground-state atom and a perfectly conducting surface at a distance r can be derived [6] from the knowledge of the (complex) frequency-dependent dipole polarizability $\alpha_d(i\omega)$ of the atom, and it is given by [23]

$$V_{\mathrm{CvdW}}^{(\infty)}(r) = \frac{-1}{4\pi\alpha_{\mathrm{fs}}r^4}\int_0^\infty \alpha_d\left(\frac{i\xi}{\alpha_{\mathrm{fs}}r}\right)e^{-2\xi}(2\xi^2 + 2\xi + 1)d\xi,$$

(25)

where $\alpha_{\mathrm{fs}} = e^2/(\hbar c)$ is the fine-structure constant. A similar formula for a dielectric surface is given in [10]. The asymptotic behavior for small and large distances is

$$V_{\mathrm{CvdW}}(r) \overset{r\to 0}{\sim} -\frac{C_3}{r^3} = -\frac{\hbar^2}{2M}\frac{\beta_3}{r^3},$$

$$V_{\mathrm{CvdW}}(r) \overset{r\to\infty}{\sim} -\frac{C_4}{r^4} = -\frac{\hbar^2}{2M}\frac{(\beta_4)^2}{r^4}.$$

(26)

The strength parameters governing the short-distance and the long-distance behavior of the potential are [23]

$$C_3 = \frac{1}{4\pi}\int_0^\infty \alpha_d(i\omega)d\omega, \quad C_4 = \frac{3}{8\pi}\frac{\alpha_d(0)}{\alpha_{\mathrm{fs}}} = 16.36\alpha_d(0).$$

(27)

The exact Casimir–van der Waals potential between a hydrogen atom and a conducting surface has been calculated numerically and tabulated by Marinescu *et al.* [23], and these authors also give approximate results, based on a one-electron model potential, for alkali-metal atoms as projectiles. The strength parameters C_3 and C_4 applying for the various potentials in Ref. [23] are listed in Table II.

In Eq. (26) we now have two quantum-mechanical length parameters, β_3 and β_4, defining the potential strength; they are usually quite large, typically of the order of many thousands of Bohr radii, see Table II. In the upper of the equations (26), $r\to 0$ means r values small compared to β_3 and β_4, but of course the interaction between the atom and the surface necessarily becomes more complicated at separations of a few Bohr radii. Whether or not the projectile atom can come close enough to the surface to interact via these short-ranged forces, resulting in inelasic scattering or adsorption ("sticking"), depends on whether the atom is transmitted or reflected by the potential tail (26).

TABLE II. Potential parameters determining the short-distance and the long-distance behavior of the Casimir–van der Waals potentials given by Marinescu *et al.* [23] for the interaction of hydrogen or various alkali-metal atoms with a perfectly conducting surface, see Eq. (26). The calculations for the alkali-metal atom projectiles are based on a one-electron model potential. The first two rows list the strength parameters C_3 and C_4 in atomic units. The next two rows show the corresponding lengths β_3 and β_4 in units of the Bohr radius. The last two rows give the length l [Eq. (28)] (in Bohr radii), which sets a scale separating the short- and long-distance regimes, and the crucial parameter ρ [Eq. (44)], which determines the relative importance of the $-1/r3$ and the $-1/r4$ parts of the potential.

	H	Li	Na	K	Rb	Cs
C_3	0.250	1.447	1.576	2.153	2.291	2.589
C_4	73.62	2683	2662	4789	5221	6579
β_3	919	3.661×10^4	1.321×10^5	3.069×10^5	7.139×10^5	1.255×10^6
β_4	520	8.239×10^3	1.494×10^4	2.613×10^4	4.033×10^4	5.646×10^4
l	294	1854	1690	2225	2278	2540
ρ	1.77	4.44	8.84	11.75	17.70	22.23

A. Scaling

In contrast to the homogeneous potentials (7), the potential tail (26) contains an energy-independent intrinsic length,

$$l = \frac{C_4}{C_3} = \frac{(\beta_4)^2}{\beta_3}, \tag{28}$$

which naturally defines a scale separating the large-r region, $r \gg l$, from the small-r region, $r \ll l$. It seems useful to express the distance coordinate r in units of this length, i.e., in terms of the dimensionless variable $x = r/l$. We also introduce the strength parameter K_0,

$$\frac{\hbar^2 (K_0)^2}{2M} \stackrel{\text{def}}{=} \frac{C_3}{l^3} = \frac{C_4}{l^4}, \tag{29}$$

so the full Casimir–van der Waals potential can be written as

$$V_{\text{CvdW}}(r) = \frac{\hbar^2 (K_0)^2}{2M} v\left(\frac{r}{l}\right), \tag{30}$$

and the asymptotic behavior (26) of $V_{\text{CvdW}}(r)$ translates into the following behavior of the dimensionless "shape function" $v(x)$,

$$v(x) \sim \begin{cases} -1/x^3 & \text{for} \quad x \to 0, \\ -1/x^4 & \text{for} \quad x \to \infty. \end{cases} \tag{31}$$

The limiting behavior (26) is fixed by any two of the four parameters β_3, β_4, l, K_0 and the other two can be expressed in terms of those. For example,

$$K_0 = \sqrt{\frac{\beta_3}{l^3}} = \frac{(\beta_3)^2}{(\beta_4)^3}, \quad K_0 l = \frac{\beta_3}{\beta_4} = \sqrt{\frac{\beta_3}{l}} = \frac{\sqrt{2M}}{\hbar} \frac{C_3}{\sqrt{C_4}}. \tag{32}$$

With the definitions (28) and (29), the Schrödinger equation with the Casimir–van der Waals potential (30) is

$$\left[\frac{d^2}{dr^2} + k^2 + (K_0)^2 v\left(\frac{r}{l}\right) \right] \psi(r) = 0. \tag{33}$$

Except for the case of hydrogen atom projectiles, we do not know exactly the shape of the potential between the two limits of large and short distances. Shimizu's [8] recent analysis of neon atoms specularly reflected by a silicon or a glass surface was based on the simple shape function

$$v_1(x) = -\frac{1}{x^3 + x^4}. \tag{34}$$

The corresponding full potential (30) is

$$V_1(r) = -\frac{C_4}{(r+l)r^3}, \tag{35}$$

showing that the length l can be identified with $\lambda/2\pi$, where λ is the effective atomic transition wavelength that contributes to the polarizability of the atom [8]. A smoother transi-
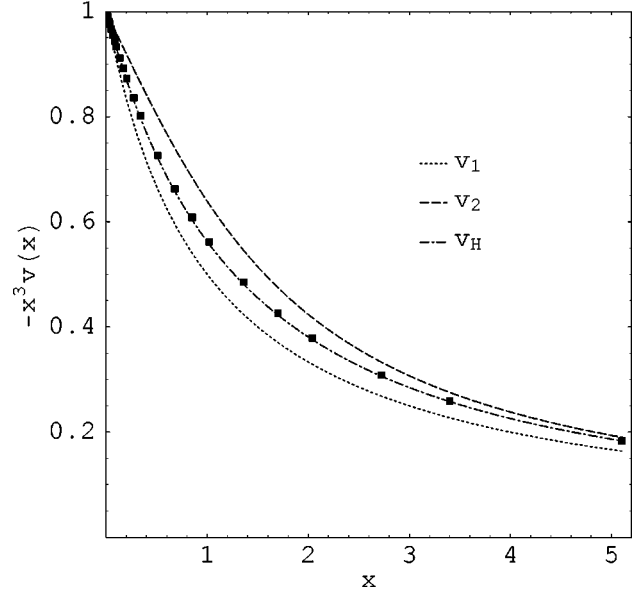
FIG. 3. Shape functions $v_1(x)$ [Eq. (34)] (dotted line), $v_2(x)$ [Eq. (36)] (dashed line), and $v_H(x)$ [Eq. (37)] (dot-dashed line). The plotted quantity is $-x^3 v(x)$ in all cases. The shape function $v_H(x)$ reproduces the values corresponding to the exact hydrogen-surface interaction tabulated by Marinescu *et al.* [23] (solid boxes) to within a maximum relative error of 0.7%.

tion from small to large x values is described with the help of an arcus tangent as used by Holstein [24] in a review of the Casimir–van der Waals potentials between two atoms. Adapted for our present purposes, this corresponds to the shape function

$$v_2(x) = -\frac{1}{x^3} \frac{2}{\pi} \arctan\left(\frac{\pi}{2x}\right). \tag{36}$$

Figure 3 shows the functions $-x^3 v_{1,2}(x)$ which start at unity for $x = 0$ and behave as $1/x$ for large x.

The shape of the exact hydrogen-surface potential tabulated in [23] lies between the two shapes (34) and (36). We have constructed a rational approximation $v_H(x)$, which reproduces the exact potential to within a maximum relative error of 0.7%,

$$v_H(x) = -\frac{1}{x^3} \left(\frac{1 + 0.22x}{1 + 0.95x + 0.22x^2} \right). \tag{37}$$

TABLE III. Parameters for the shape function (38) for the Casimir–van der Waals potentials between alkali-metal atoms and a conducting surface. The potentials defined via Eqs. (30) and (38) with these shapes and the strength parameters of Table II reproduce the potentials obtained by Marinescu *et al.* [23] on the basis of a one-electron model potential to within a maximum relative error of less than 0.6% in all cases.

	Li	Na	K	Rb	Cs
ζ	0.3	0.35	0.4	0.4	0.41
η	0.98	0.98	1	1	1

TABLE IV. Results of more sophisticated determinations [25–27] of the van der Waals parameter C_3 of the alkali-surface interaction.

Li [25]	Na [26]	K [27]	Rb [27]	Cs [27]
1.518	1.889	2.86	3.36	4.14

The shape function v_H is also shown in Fig. 3, and the filled boxes show the values corresponding to the exact potential tabulated in [23].

The expression

$$v_X(x) = -\frac{1}{x^3}\left(\frac{1+\zeta x}{1+\eta x+\zeta x^2}\right) \tag{38}$$

can also be used to approximate the shapes of the alkali-surface potentials given by Marinescu *et al.* in [23]. The functions defined with the parameters η and ζ listed in Table III reproduce the respective alkali-surface potentials of [23] within a maximum relative error of less than 0.6% in all cases. The similarity of the parameters ζ and η obtained for the various atoms in Table III shows that the shape functions for the alkali-surface potentials based on one-electron model potentials are all actually quite similar.

Further effort has since gone into more sophisticated determinations of the parameters of alkali-surface interactions, in particular of the van der Waals coefficient C_3 [25–27]. A list of these more recent C_3 values is given in Table IV.

B. Near-threshold reflectivities

Since the Casimir–van der Waals potential falls off faster than $1/r^2$ for large r, the near-threshold reflectivity is given by Eq. (4) or, as it turns out, more accurately by Eq. (12). The parameter b depends on the potential tail, i.e., on the length parameters β_3 and β_4 and on the shape function $v(x)$. For the shape function (34), the Schrödinger equation (33) possesses analytical solutions at threshold ($k=0$) [28]. The solutions behaving asymptotically ($r\to\infty$) as $\psi_0(r)\sim 1$ and $\psi_1(r)\sim r$ are

$$\psi_{0,1} = \sqrt{r(r+l)}[A_{0,1}J_1(z)+B_{0,1}Y_1(z)], \quad z = 2\sqrt{\frac{\beta_3}{r}+\frac{\beta_3}{l}}, \tag{39}$$

where J_1 and Y_1 are the ordinary Bessel functions of order unity [18], and the coefficients $A_{0,1}, B_{0,1}$ are

$$A_0 = -\frac{\pi}{l}Y_1(2K_0l), \quad B_0 = \frac{\pi}{l}J_1(2K_0l),$$

$$A_1 = \pi(K_0lY_1'(2K_0l)+\tfrac{1}{2}Y_1(2K_0l)), \tag{40}$$

$$B_1 = -\pi(K_0lJ_1'(2K_0l)+\tfrac{1}{2}J_1(2K_0l)).$$

Casting the small-r behavior of the wave functions (39) into the WKB form (5) yields the amplitudes

$$D_{0,1} = \sqrt{\hbar l}\sqrt{(A_{0,1})^2+(B_{0,1})^2} \tag{41}$$

and the phases

$$\phi_{0,1} = \frac{3}{2}\pi - 4K_0l + 2\arctan\frac{B_{0,1}}{A_{0,1}}, \tag{42}$$

so the length b determining the near-threshold reflectivity is, according to Eq. (6),

$$b_{v_1} = \frac{l/\pi}{J_1(2K_0l)^2+Y_1(2K_0l)^2}. \tag{43}$$

The properties of the reflectivity depend crucially on the parameter

$$\rho \overset{\text{def}}{=} K_0l = \frac{\beta_3}{\beta_4} = \frac{\sqrt{2M}}{\hbar}\frac{C_3}{\sqrt{C_4}}. \tag{44}$$

This is clear from Eq. (43) for the near-threshold behavior with the shape function (34), but it is also true for other potential shapes and beyond the near-threshold region, as will be shown below.

For large values of ρ, we have $J_1(2\rho)^2+Y_1(2\rho)^2 \to 1/(\pi\rho)$ and $b_{v_1}\to\rho l=\beta_4$. For small values of ρ, $J_1(2\rho)^2+Y_1(2\rho)^2\to 1/(\pi\rho)^2$ and $b_{v_1}\to\pi\rho^2l=\pi\beta_3$. These limits are consistent with the results (9) for homogeneous potentials, because the Casimir–van der Waals potential is dominated by the $-1/r^3$ behavior when $\beta_3\ll\beta_4$ and by the $-1/r^4$ behavior when $\beta_4\ll\beta_3$. This perhaps counterintuitive observation is readily understandable when we write the potential (35) in the form

$$V_1(r) = -\frac{\hbar^2}{2M}\left[\frac{r^3}{\beta_3}+\frac{r^4}{(\beta_4)^2}\right]^{-1}. \tag{45}$$

The dependence of the length parameter (43) on ρ is shown in Fig. 4. The dotted lines show both the ratio b_{v_1}/β_3 [part (a)], which approaches the value π (appropriate for a homogeneous $-1/r^3$ potential) in the limit $\rho\to 0$, and the ratio b_{v_1}/β_4 [part (b)], which approaches unity (appropriate for a homogeneous $-1/r^4$ potential) in the limit $\rho\to\infty$.

For the shape functions (36) and (37), the zero-energy solutions of the Schrödinger equation (33) are not known analytically, so we derived the near-threshold behavior of the reflectivity by numerically solving Eq. (33). The length parameter b was obtained by fitting the reflectivity to the exponential form (12) in the limit $k\to 0$, and the results are shown in Fig. 4 as dashed [shape function v_2, Eq. (34)] and dot-dashed lines [shape function v_H, Eq. (37)], respectively.

Figure 4 illustrates the transition of the near-threshold reflectivity from the expectations for a $-1/r^3$ potential for small values of $\rho=\beta_3/\beta_4$ to those of a $-1/r^4$ potential for large values of ρ. It also illustrates how this transition depends on the shape function $v(x)$. For the shape function (34), b_{v_1}/β_4 depends monotonically on ρ and approaches

(a)

(b)
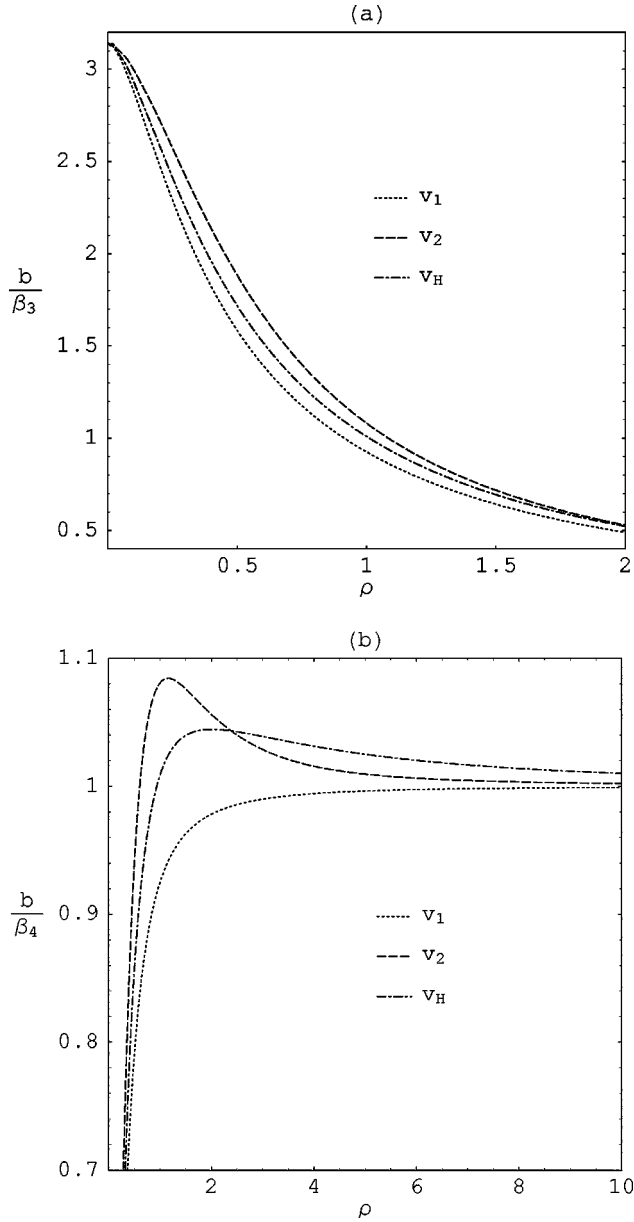
FIG. 4. Length parameters b determining the near-threshold reflectivities of Casimir–van der Waals potential tails according to Eq. (12). Part (a) shows the ratio b/β_3, which would be π according to Eq. (9) for a homogeneous $-1/r^3$ potential; part (b) shows the ratio b/β_4, which would be unity for a homogeneous $-1/r^4$ potential. The dotted lines give the analytical results (43) for the shape function (34) and the dashed lines give the numerical results obtained for the shape function (36). The dot-dashed lines give the numerical results obtained for the shape function (37) describing the hydrogen-surface potential tabulated in [23].

the large-ρ limit from below. For the other shapes (36) and (37), b approaches β_4 from above, and the ratio b/β_4 remains greater than unity all the way down to $\rho \approx 1$. The largest differences in b due to the different potential shapes are seen around $\rho \approx 1$. The ratio b_{v_2}/b_{v_1} has a maximum value of 1.19 for $\rho = 0.63$. The value of b_H differs from b_{v_2} or b_{v_1} by less than 10%.

C. Beyond the near-threshold region

For high energies, the badlands function (3) becomes smaller and smaller and more and more concentrated around small r values (see the Appendix). The maximum of the badlands function is close to the point r_0 where the absolute value of the potential equals the total energy. If this point lies well in the small-r domain of the Casimir–van der Waals potential, i.e., if $r_0 \ll l$, then the potential behaves like a homogeneous potential (7) with $\alpha = 3$ around r_0, and we expect the reflectivity to be given by Eq. (17),

$$|R_{CvdW}| \overset{k\to\infty}{\sim} \exp[-B_3(k\beta_3)^{1/3}], \quad B_3 = 2.2405. \quad (46)$$

Inserting (15) with $\alpha = 3$ for r_0 into the condition $r_0 \ll l$ leads to $k^{-2/3}(\beta_3)^{1/3} \ll l$, so the energy range where we expect Eq. (46) to hold is given by

$$k\beta_3 \gg \left(\frac{\beta_3}{l}\right)^{3/2} = \rho^3. \quad (47)$$

For small values of ρ, the condition $k\beta_3 \gg 1$ is also needed, because Eq. (46) refers to the high-energy behavior in a $-1/r^3$ potential and is, of course, not valid in the near-threshold region.

The behavior (46) will always be reached for sufficiently high energies, but if ρ is large, the reflectivity may be dominated by the $-1/r^4$ nature of the potential, not only in the near-threshold region but also for larger energies, where the asymptotic behavior (17) already applies — for $\alpha = 4$,

$$|R_{CvdW}| \approx \exp[-B_4(k\beta_4)^{1/2}], \quad B_4 = 1.694\,43. \quad (48)$$

For Eq. (48) to hold, the point r_0 where the absolute value of the potential equals the total energy should lie in the large-r domain, $r_0 \gg l$. Inserting Eq. (15) with $\alpha = 4$ into this condition yields $\sqrt{k} \ll \sqrt{\beta_4}/l = \beta_3/(\beta_4)^{3/2}$. We can thus expect the reflectivity to be given by Eq. (48) in the energy range defined by

$$1 \ll k\beta_4 \ll \left(\frac{\beta_3}{\beta_4}\right)^2 = \rho^2, \quad (49)$$

where the first inequality ensures that the range lies far enough beyond the near-threshold region.

The overall behavior of the reflectivity is thus characterized by a linear dependence of $-\ln|R_{CvdW}|$ on k near threshold, Eq. (12), which changes to proportionality to $k^{1/3}$ at high energies (46). How this transition occurs depends essentially on the parameter $\rho = \beta_3/\beta_4$. For very small values of ρ, the reflectivity corresponds to that of a $-1/r^3$ potential (see Sec. II, Figs. 1 and 2) in the whole range from threshold to the high-energy limit. For sufficiently large values of ρ, there is a range of energies defined by Eq. (49), where we expect the reflectivity to be given by Eq. (48). For sufficiently high energy, the reflectivity will eventually be given by Eq. (46).

Figure 5 shows $\ln(-\ln|R_{CvdW}|)$ as a function of $\ln(k\beta_3)$ for a small value of ρ, namely $\rho = \frac{1}{10}$. The three curves correspond to the three shape functions (34) (dotted line), (36) (dashed line), and (37) (dot-dashed line). The respective val-
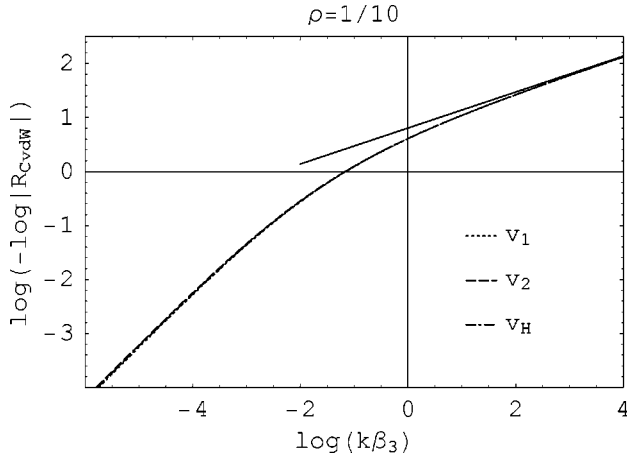
FIG. 5. Reflectivities $|R_{\mathrm{CvdW}}|$ of Casimir–van der Waals potentials for $\rho = \frac{1}{10}$. The results for the three shape functions (34), (36), and (37) are shown as (hardly distinguishable) dotted, dashed, and dot-dashed lines, respectively. The straight solid line shows the high-energy behavior expected for a homogeneous $-1/r^3$ potential according to Eq. (46).

ues of the length b determining the near-threshold reflectivity according to Eq. (12) are given by $b/(\pi\beta_3) = 0.916,\ 0.954,$ and 0.933, showing that the near-threshold behavior depends only weakly on the shape of the potential and is already quite close to the expectation for a $-1/r^3$ potential. The reflectivity in fact behaves much like that of a $-1/r^3$ potential in the whole range of energies and merges into the straight line of gradient $\frac{1}{3}$ corresponding to the high-energy behavior Eq. (46).

Figure 6 shows $\ln(-\ln|R_{\mathrm{CvdW}}|)$ as a function of $\ln(k\beta_3)$ for $\rho = 1$, which implies $\beta_3 = \beta_4$. The results obtained for the three shape functions (34), (36), and (37) are again shown as
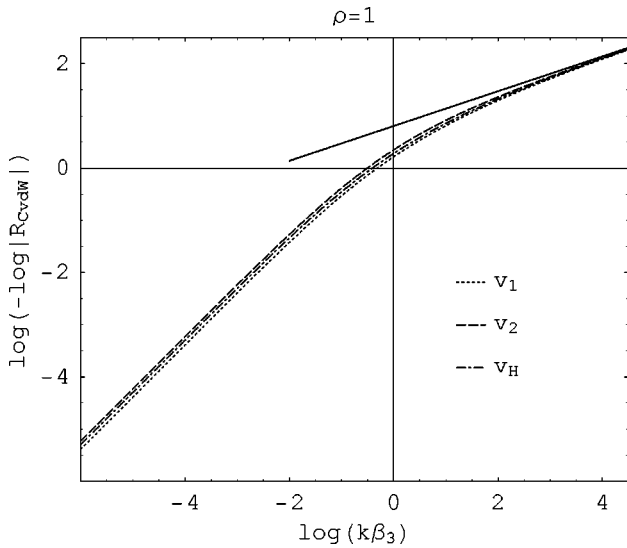
FIG. 6. Reflectivities $|R_{\mathrm{CvdW}}|$ of Casimir–van der Waals potentials for $\rho = 1$. The three curves correspond to the shape functions (34) (dotted line), (36) (dashed line), and (37) (dot-dashed line). The straight solid line shows the high-energy behavior expected for a straight solid line shows the high-energy behavior expected for a homogeneous $-1/r^3$ potential according to Eq. (46).
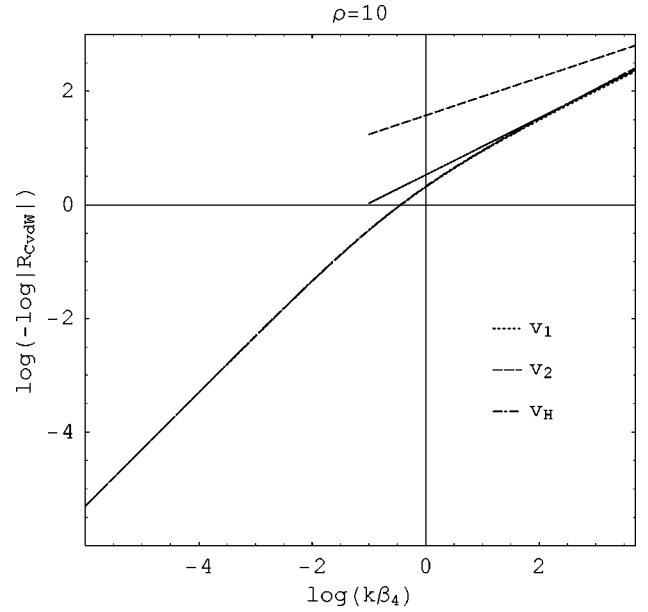
FIG. 7. Reflectivities $|R_{\mathrm{CvdW}}|$ of Casimir–van der Waals potentials for $\rho = 10$. The results for the three shape functions (34), (36), and (37) are shown as (hardly distinguishable) dotted, dashed, and dot-dashed lines, respectively. The straight solid line shows the high-energy behavior expected for a homogeneous $-1/r^4$ potential according to Eq. (48); the straight dashed line shows the high-energy behavior expected for a homogeneous $-1/r^3$ potential according to Eq. (46).

dotted, dashed, and dot-dashed lines, respectively. The b value determining the near-threshold reflectivity shows a larger dependence on the potential shape and is given by $b/\beta_4 (= b/\beta_3) = 0.925,\ 1.081,$ and 1.009 for the three cases. The curves in Fig. 6 show a more gradual transition from a straight line of unit gradient describing the near-threshold behavior (12) to the straight line of gradient $\frac{1}{3}$ corresponding to the high-energy behavior in a $-1/r^3$ potential, Eq. (46).

Figure 7 shows $\ln(-\ln|R_{\mathrm{CvdW}}|)$ for $\rho = 10$, which implies $\beta_3 = 10\beta_4$. Again the dotted, dashed, and dot-dashed lines correspond to the three shape functions (34), (36), and (37), but the dependence on shape is now very small. The b value determining the near-threshold reflectivity is given by $b/\beta_4 = 0.999,\ 1.002,$ and 1.010, respectively. For values of $\ln(k\beta_4)$ near and above 2, the curves are close to the straight (solid) line of gradient $\frac{1}{2}$ corresponding to the high-energy behavior in a $-1/r^4$ potential [Eq. (48)]. The high-energy behavior in a $-1/r^3$ potential is shown as a straight dashed line, and it lies somewhat above the curves and the straight solid line in Fig. 7.

The transition from the (high-energy) behavior (48) appropriate for a homogeneous $-1/r^4$ potential to that of a homogeneous $-1/r^3$ potential (46) may be expected near the point where the two lines defined by Eqs. (48) and (46) intersect, i.e., where $B_4(k\beta_4)^{1/2} = B_3(k\beta_3)^{1/3}$. This point is given by

$$\frac{k}{K_0} = \frac{k\beta_4}{\rho^2} = \frac{k\beta_3}{\rho^3} = \left(\frac{B_3}{B_4}\right)^6 = 5.345, \qquad (50)$$

and it lies in between the range of energies fulfilling Eq. (49) and the range fulfilling Eq. (47). At the point of intersection (50), the reflectivity (46) of the homogeneous $-1/r^3$ potential and the reflectivity (48) of the homogeneous $-1/r^4$ potential (both in the high-energy limit) are equal and given by

$$|R_{\mathrm{intersect}}| = \exp(-B_4(k\beta_4)^{1/2}) = \exp(-B_3(k\beta_3)^{1/3})$$
$$= \exp(-3.92\rho). \tag{51}$$

The reflectivities are, of course, not necessarily given accurately by the expressions (46) and/or (48) for energies in the transition region, but the value (51) can be used as a guide for the order of magnitude of the reflectivity near the energy defined by Eq. (50).

For the case shown in Fig. 7, $\rho=10$, the transition is expected for $k\beta_4 \approx 530$, $\ln(k\beta_4) \approx 6.3$, which is well outside the range of the figure. The value of $|R_{\mathrm{intersect}}|$ [Eq. (51)] is near 10^{-17} at this value of k, so the transition from the $-1/r^4$ behavior to the $-1/r^3$ behavior can be expected at very small reflectivities indeed. For the range covered in Fig. 7, the reflectivities are essentially those of a homogeneous $-1/r^4$ potential, see Fig. 2.

IV. ILLUSTRATION

Shimizu [8] recently presented experimental data for the reflectivity of neon atoms scattered from a silicon or a glass surface. He fitted the observed data to the reflectivities obtained by solving the Schrödinger equation with the potential (35) and concluded that the data revealed manifestations of the Casimir effect, because a $-1/r^4$ contribution in the potential was needed to reproduce the energy dependence of the observed reflectivities. The importance of the Casimir effect can be illustrated more directly, by plotting the data in the style of Figs. 2 and 5–7 above.

Figure 8 shows (in atomic units) the experimental data of Shimizu for reflection by the silicon surface. We have plotted $\ln(-\ln|R|)$ as a function of $\ln k$. At the high-energy end of the figure, the data clearly approximate a straight line with a gradient near $\frac{1}{2}$, which is the signature of the high-energy behavior in a $-1/r^4$ potential. Fitting a straight line through the last six to ten data points yields gradients ranging from 0.45 to 0.55. Fitting a straight line of gradient $\frac{1}{2}$ through the last six to ten data points yields

$$\ln(-\ln|R|) = 5.2 + \frac{1}{2}\ln k. \tag{52}$$

The straight line (52) is shown in the top right-hand part of the figure. Comparing this with Eq. (48),

$$\ln(-\ln|R|) = \ln B_4 + \frac{1}{2}\ln k + \frac{1}{2}\ln\beta_4 \tag{53}$$

determines the strength parameter β_4 governing the long-distance part of the potential to be $\beta_4 = \exp[2(5.2 - \ln B_4)] = 11\,400a_0$. This compares favorably with the number $\beta_4 = 12\,100a_0$ corresponding to the value 6.7×10^{-56} J m^4 which Shimizu gives for C_4. The data in Fig. 8 clearly do not
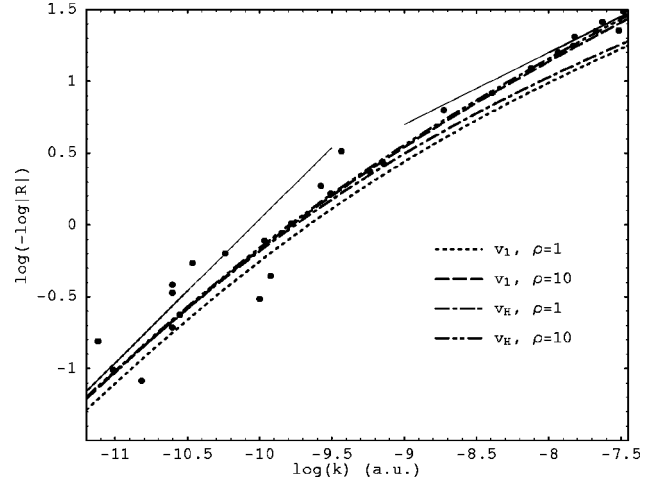
FIG. 8. Reflectivities $|R|$ as observed by Shimizu [8] for the scattering of neon atoms by a silicon surface (filled dots). The figure shows $\ln(-\ln|R|)$ as a function of $\ln k$. The straight solid line in the top right-hand part of the figure shows the high-energy behavior expected for a homogeneous $-1/r^4$ potential according to Eq. (48) for $\beta_4 = 11\,400$. The straight solid line in the bottom left-hand part of the figure shows the near-threshold behavior (12) for $b = \beta_4 = 11\,400$. The curves were calculated by solving the Schrödinger equation with the shape functions v_1 (34) or v_H (37) for the above value of β_4, and $\rho=10$ ($\beta_3 = 10\beta_4$) or $\rho=1$ ($\beta_3 = \beta_4$).

reach energies high enough for the $-1/r^3$ part of the potential to become important. This indicates that we are in the regime of large ρ, $\beta_4 \ll \beta_3$, which is confirmed by comparing with the reflectivities calculated by solving the Schrödinger equation with the above value of β_4 ($11\,400a_0$) and $\rho=10$. In contrast, the reflectivities obtained using $\rho=1$ (dotted and dot-dashed lines in Fig. 8) deviate significantly from the data towards the high-energy end of the range covered in the figure. Within this range, the reflectivities obtained for $\rho=10$ are essentially those of a homogeneous $-1/r^4$ potential (corresponding to $\rho \to \infty$), as already discussed in connection with Fig. 7 above. Thus the data in Fig. 8 are not suitable for deducing an upper limit on ρ or, equivalently, a lower limit on the length $l = \beta_4/\rho$; this is consistent with the value $l \approx 0$ quoted by Shimizu.

For such large values of ρ, the length parameter b determining the near-threshold behavior (12) of $|R|$ is essentially equal to β_4, see Fig. 4. The straight line

$$\ln(-\ln|R|) = \ln(2\beta_4) + \ln k \tag{54}$$

is shown in the bottom left-hand part of Fig. 8; it fits in quite well with the low-energy behavior of the data, but their scatter is very large.

V. DISCUSSION

The parameter ρ defined by Eq. (44) is the crucial quantity which determines how important the $-1/r^3$ and the $-1/r^4$ parts of the Casimir–van der Waals potential are for quantum reflection. For $\rho \ll 1$, the reflectivities are essentially those of a homogeneous $-1/r^3$ potential, and they are unaf-

fected by the retardation effects in the potential. For moderate and large values of ρ, the behavior appropriate for a homogeneous $-1/r^3$ potential sets in for $k\beta_3 \gg \rho^3$ [Eq. (47)]. If ρ is sufficiently large, then there is a regime of lower energies corresponding to $k\beta_4 \ll \rho^2$ [Eq. (49)], where the reflectivities are essentially those of a homogeneous $-1/r^4$ potential and depend only on the strength parameter β_4 (i.e., C_4) of the Casimir–van der Waals potential. In the energy range defined by $1 \ll k\beta_4 \ll 5\rho^2$, the reflectivities behave as given by Eq. (48), and this shows up as a straight line of gradient $\frac{1}{2}$ in a plot of $\ln(-\ln|R|)$ against $\ln k$. This is a conspicuous and model-independent signature of retardation effects in the potential and can be used to determine the parameter β_4, i.e., the strength C_4, of the $-1/r^4$ part of the potential, as illustrated in Sec. IV.

The transition between the $-1/r^4$ and the $-1/r^3$ regimes can be expected near the energy given by Eq. (50), $(k\beta_4)^{1/2} \approx 2.3\rho$, $(k\beta_3)^{1/3} \approx 1.75\rho$, and for reflectivities near $|R| \approx \exp(-4\rho)$, see Eq. (51). For moderate values of ρ and for energies below the "transition point" given by Eq. (50), the reflectivities depend on both β_4 and β_3, and on the shape of the potential in between the long- and short-distance regimes. In the near-threshold region, $|R|$ is given by $\exp(-2bk)$, and b depends (for moderate ρ values) significantly on ρ and the potential shape, see Fig. 4.

The strength parameters C_3 and C_4 defining the short- and long-distance parts of the Casimir–van der Waals potential are determined by the dipole polarizability of the projectile atom, see Eq. (27). The polarizability depends on the electronic structure of the atom and so C_3 and C_4 can be expected to be similar for similar electronic configurations. This is confirmed by Table I, where the values of C_3 and C_4 agree to within a factor of 2.5 for the alkali-metal atoms from Li to Cs. The crucial parameter ρ is given by $\rho = (\sqrt{2M}/\hbar)(C_3/\sqrt{C_4})$, see Eq. (44), so for given values of C_3 and C_4 we obtain small ρ values for small masses and large ρ values for large masses. A reflectivity behaving as for a homogeneous $-1/r^4$ potential, as a conspicuous and model-independent signature of the Casimir effect, is thus most likely to be observed for heavy projectiles. Of course, the energy where appreciable (observable) reflection occurs is then correspondingly small.

Large values of ρ are ubiquitous in realistic systems, see, e.g., Table I and the above data for neon atoms reflected by a silicon surface. This means that quantum reflection of atoms is quite generally dominated by the retardation effects in the Casimir–van der Waals potential. The transition (50) between the $-1/r^4$ and the $-1/r^3$ regimes occurs for extremely small reflectivities when ρ is large. Information about the short-distance part of the potential, i.e., about the parameter β_3 and/or the shape of the potential, is more readily obtained in systems with small or moderate ρ values. These can be achieved by choosing light projectiles or surfaces with small dielectric constants, which reduces the strength of the whole potential [10] and also the ratio $C_3/\sqrt{C_4}$.

ACKNOWLEDGMENT

APPENDIX

The accuracy of the WKB approximation is a local property of the Schrödinger equation. First-order WKB wave functions (1) are accurate solutions of the Schrödinger equation when the condition (3) is fulfilled [11,12,22]. The frequently quoted simpler condition [4,8,16]

$$\left| \frac{d}{dr}\left(\frac{\hbar}{p(r)} \right) \right| = \hbar \left| \frac{p'}{p^2} \right| \ll \frac{1}{2\pi} \qquad (A1)$$

often works too, but in general it is neither necessary nor sufficient. The example of a potential proportional to $1/r^4$ shows that it is not necessary: for zero energy, first-order WKB wave functions are exact solutions of the Schrödinger equation for all r, but the left-hand side of Eq. (A1) is proportional to r and grows to infinity for $r \to \infty$. Note that the badlands function defined by Eq. (3) vanishes in this example. To see that the condition (A1) is not sufficient, consider a particle with a moderate kinetic energy over a potential with oscillations of small scale and amplitude. For an appropriate potential we could have, e.g., $\hbar/p(r) = 1 + \sin(qr)/q^{3/2}$, and the left-hand side of Eq. (A1) would be $|\cos(qr)|/\sqrt{q}$, which becomes arbitrarily small as $q \to \infty$. However, the term involving the p''/p^3 in the badlands function (3) contains a contribution which is proportional to $\sqrt{q}\sin(qr)$ and becomes larger and larger for $q \to \infty$.

Mody $et\ al.$ [4] point out that quantum reflection is generated in the region where the WKB approximation breaks down, and they observe that this occurs mainly near the point r_0, where the absolute value of the potential energy is equal to the (asymptotic) kinetic energy, i.e., the total energy

$$|V(r_0)| = E = \frac{\hbar^2 k^2}{2M}. \qquad (A2)$$

For the homogeneous potential tail (7), we have [see Eq. (15)]

$$r_0 = k^{-2/\alpha}(\beta_\alpha)^{1-2/\alpha}. \qquad (A3)$$

The maximum of the left-hand side of Eq. (A1), however, occurs for [4,8]

$$\frac{\hbar^2 k^2}{2M} = |V(r)|\frac{\alpha - 2}{2\alpha + 2} \qquad (A4)$$

corresponding to

$$r = \left(\frac{\alpha - 2}{2\alpha + 2} \right)^{1/\alpha} r_0. \qquad (A5)$$

This is smaller than the position r_0 defined by Eqs. (A2) and (A3) by a factor of 2 for $\alpha = 3$ and 1.5 for $\alpha = 4$.

For the homogeneous potential tail (7), the badlands function (3) is
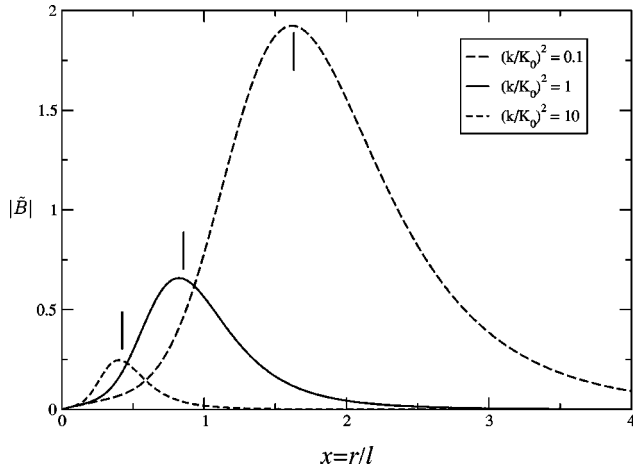
FIG. 9. Scaled badlands function $\widetilde{B}$ as defined by Eqs. (3) and (A10) as function of the dimensionless coordinate $x=r/l$ for scaled energies $(k/K_0)^2=0.1$ (long dashed line), 1.0 (solid line), and 10 (short dashed line). The shape function is that of Eq. (37) approximating the exact hydrogen-surface interaction. The vertical bars mark the points $x_0=r_0/l$ where the condition (A2) is fulfilled at the respective (scaled) energies.

$$B(r)=\frac{5\alpha^2(\beta_\alpha)^{2\alpha-4}}{16r^{2\alpha+2}[k^2+(\beta_\alpha)^{\alpha-2}/r^\alpha]^3}$$

$$-\frac{\alpha(\alpha+1)(\beta_\alpha)^{\alpha-2}}{4r^{\alpha+2}[k^2+(\beta_\alpha)^{\alpha-2}/r^\alpha]^2}, \qquad (A6)$$

and maxima of $|B(r)|$ occur when

$$k^2=F(\alpha)\frac{(\beta_\alpha)^{\alpha-2}}{r^\alpha},$$

$$F(\alpha)=\frac{5}{4}-\frac{9}{2\alpha+4}\pm\frac{9\alpha}{4\alpha+8}\sqrt{1-\frac{20}{27}\left(\frac{\alpha+2}{\alpha+1}\right)}. \quad (A7)$$

The positions of these maxima are

$$r_{\mathrm{max}}=[F(\alpha)]^{1/\alpha}r_0, \qquad (A8)$$

with r_0 as given by Eq. (A3). For $\alpha>4$, the function $B(r)$ has a zero at $r=\frac{1}{4}[1-5/(\alpha+1)]^{1/\alpha}r_0$; there is a larger maximum of $|B|$ above and a smaller one below this zero. For $\alpha=3,4$, only the plus sign before the square root in Eq. (A7) yields a positive value of $F(\alpha)$, namely $F(3)=0.7174$ and $F(4)=1$, so $r_{\mathrm{max}}=0.895r_0$ for $\alpha=3$ and $r_{\mathrm{max}}=r_0$ for $\alpha=4$. The conjecture that reflection occurs mainly in the region (A2) is justified more readily on the basis of the badlands function (3) than via the simpler condition (A1).

For the Casimir–van der Waals potential(s), the expression for the badlands function is more complicated, but the small-r and the large-r behavior follow from Eq. (A6) for $\alpha=3$ and $\alpha=4$, respectively,
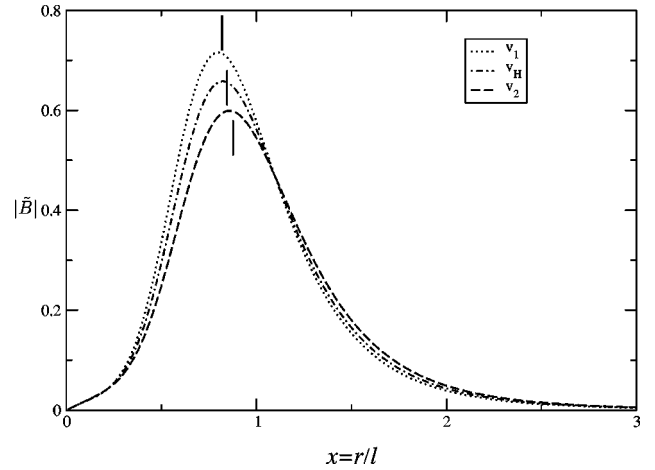
FIG. 10. Scaled badlands function $\widetilde{B}$ as defined by Eqs. (3) and (A10) as a function of the dimensionless coordinate $x=r/l$ for the three shape functions v_1 [Eq. (34), dotted line], v_2 [Eq. (36), dashed line], and v_H [Eq. (37), dot-dashed line]. The scaled energy is $(k/K_0)^2=1$ and the vertical bars mark the points $x_0=r_0/l$ where the condition (A2) is fulfilled for the various potentials.

$$B(r)\overset{r\to 0}{\sim}-\frac{3}{16}\frac{r}{\beta_3}, \quad B(r)\overset{r\to\infty}{\sim}-\frac{5(\beta_4)^2}{k^4r^6}. \qquad (A9)$$

The dependence of $B(r)$ on the strength parameters of the potential can be scaled out by writing

$$B(r)=\frac{1}{\rho^2}\widetilde{B}\left(\frac{r}{l},\frac{k}{K_0}\right), \qquad (A10)$$

where l and K_0 are the parameters introduced in Sec. III A, see Eqs. (28), (29), and (32). The scaled badlands function $\widetilde{B}$ depends only on the scaled coordinate r/l and on the scaled (asymptotic) wave number k/K_0 [or equivalently, scaled energy $(k/K_0)^2$], and, of course, on the potential shape. The scaled badlands function is shown in Fig. 9 as a function of the dimensionless coordinate $x=r/l$ for three values of the scaled energy, namely $(k/K_0)^2=0.1$, 1.0, and 10. The shape function underlying this illustration is that of Eq. (37) approximating the exact hydrogen-surface interaction. The vertical bars mark the points $x_0=r_0/l$, where r_0 is the position fulfilling Eq. (A2) at the respective energy. The shape dependence of the badlands function is illustrated in Fig. 10 showing $\widetilde{B}$ for the three shape functions v_1 [Eq. (34)], v_2 [Eq. (36)], and v_H [Eq. (37)]. Here the scaled energy was taken as $(k/K_0)^2=1$, and the vertical bars again mark the points $x_0=r_0/l$. Figures 9 and 10 show that the position of the maximum of the badlands is (roughly) given by the condition (A2), not only for homogeneous potential tails but also for those of the Casimir–van der Waals type.

[1] V. U. Nayak, D. O. Edwards, and N. Masuhara, Phys. Rev. Lett. **50**, 990 (1983).

[2] J. J. Berkhout, O. J. Luiten, I. D. Setija, T. W. Hijmans, T. Mizusaki, and J. T. M. Walraven, Phys. Rev. Lett. **63**, 1689 (1989).

[3] I. A. Yu, J. M. Doyle, J. C. Sandberg, C. L. Cesar, D. Kleppner, and T. J. Greytak, Phys. Rev. Lett. **71**, 1589 (1993).

[4] A. Mody, M. Haggerty, J. M. Doyle, and E. J. Heller, Phys. Rev. B **64**, 085418 (2001).

[5] G. Vidali, G. Ihm, H.-Y. Kim, and M. W. Cole, Surf. Sci. Rep. **12**, 133 (1991).

[6] H. B. G. Casimir and D. Polder, Phys. Rev. **73**, 360 (1948).

[7] M. Bordag, U. Mohideen, and V. M. Mostepanenko, Phys. Rep. **353**, 1 (2001).

[8] F. Shimizu, Phys. Rev. Lett. **86**, 987 (2001).

[9] B. Segev, R. Côté and M. G. Raizen, Phys. Rev. A **56**, R3350 (1997).

[10] R. Marani, L. Cognet, V. Savalli, N. Westbrook, C. I. Westbrook, and A. Aspect, Phys. Rev. A **61**, 053402 (2000).

[11] M. V. Berry and K. E. Mount, Rep. Prog. Phys. **35**, 315 (1972).

[12] H. Friedrich *Theoretical Atomic Physics*, 2nd ed. (Springer-Verlag, Berlin, 1998).

[13] C. Eltschka, M. J. Moritz, and H. Friedrich, special issue on coherent matter waves, edited by K. Burnett, J. Phys. B **33**, 4033 (2000).

[14] J. Trost, C. Eltschka, and H. Friedrich, J. Phys. B **31**, 361 (1998).

[15] C. Eltschka, H. Friedrich, and M. J. Moritz, Phys. Rev. Lett. **86**, 2693 (2001).

[16] R. Côté, H. Friedrich, and J. Trost, Phys. Rev. A **56**, 1781 (1997).

[17] J. Trost, C. Eltschka, and H. Friedrich, Europhys. Lett. **43**, 230 (1998).

[18] M. Abramowitz and I. A. Stegun, *Handbook of Mathematical Functions* (Dover, New York, 1972).

[19] M. J. Moritz, Doctoral thesis, Technical University Munich, 2001; URL http://tumb1.biblio.tu-muenchen.de/publ/diss/ph/2001/moritz

[20] V. L. Prokovskii, S. K. Savvinykh, and F. K. Ulinich, Sov. Phys. JETP **34**, 879 (1958).

[21] V. L. Prokovskii, F. K. Ulinich, and S. K. Savvinykh, Sov. Phys. JETP **34**, 1119 (1958).

[22] N. Maitra and R. J. Heller, Phys. Rev. A **54**, 4763 (1996).

[23] M. Marinescu, A. Dalgarno, and J. F. Babb, Phys. Rev. A **55**, 1530 (1997).

[24] B. Holstein, Am. J. Phys. **69**, 441 (2001).

[25] Z.-C. Yan, A. Dalgarno, and J. F. Babb, Phys. Rev. A **55**, 2882 (1997).

[26] P. Kharchenko, J. F. Babb, and A. Dalgarno, Phys. Rev. A **55**, 3566 (1997).

[27] A. Derevianko, W. R. Johnson, M. S. Safronova, and J. F. Babb, Phys. Rev. Lett. **82**, 3589 (1999).

[28] A. D. Polyanin and V. F. Zaitsev, *Handbuch der Linearen Differentialgleichungen* (Spektrum Akad. Verlag, Heidelberg, 1996), p. 46.